The current issue and full text archive of this journal is available at
www.emeraldinsight.com/0961-5539.htm

A comparison between high-resolution central and Godunov-based schemes for the black-oil simulation

A. Karimi, H. Naderan, M.T. Manzari and S.K. Hannani
Sharif University of Technology, Tehran, Iran

Received 3 November 2007
Revised 10 December 2007
Accepted 18 December 2007

Abstract

Purpose – This paper aims to perform a comparative study between capabilities of two numerical schemes from two main branches of numerical methods for solving hyperbolic conservation equations.

Design/methodology/approach – The accuracy and performance of a newly developed high-resolution central scheme vs a higher-order Godunov-based method are evaluated in the context of black-oil reservoir simulations. Both methods are modified enabling study of applications that are not strictly hyperbolic and exhibit local linear degeneracies in their wave structure.

Findings – The numerical computations show that while both schemes produce results with virtually the same accuracy, the Godunov method reproduces slightly more accurate results at the expense of calculation of eigen-structures.

Research limitations/implications – The paper investigates only one dimensional problems, but the idea can be easily extended to multi-dimensional problems.

Practical implications – The paper shows the strengths and weaknesses of two practical numerical methods.

Originality/value – Such comparative study has not been published elsewhere and in particular, the performance of numerical methods on simulating hysteresis effect in hydrocarbon reservoirs has not been investigated in detail before.

Keywords Flow, Porous materials, Numerical analysis, Fluid mechanics

Paper type Research paper

Introduction

The multi-phase flow of multi-component fluids in porous media has been investigated extensively in recent decades in order to analyze the oil recovery process and plan for more economical exploitation (Watts, 1997). In this respect various mathematical models describing reservoir phenomena ranging from single-component single-phase flows (Aronofsky and Jenkins, 1954) to compositional multi-phase (Class *et al.*, 2002) flow models have been used. Also, the effect of matrix deformation on the behavior of multi-phase flows in reservoirs has been studied extensively and numerical techniques were developed to handle such cases (Lewis and Sukirman, 1993; Ghafouri and Lewis, 1996; Pao and Lewis, 2002).

Analysis of multi-phase multi-component flow in a reservoir is a challenging task. This is partly due to the physical and geometrical complexities that must be taken into account and partly due to the multi-scale nature of the reservoir physical properties. Study of such problems can be achieved by using appropriate numerical methods on carefully refined grids. This often makes the analysis computationally highly demanding. Such computations typically require time-steps as small as a fraction of a day to simulate processes within a specific time span in the order of several years. Moreover, the heterogeneity in physical properties of the rock frequently leads to

International Journal of Numerical Methods for Heat & Fluid Flow
Vol. 19 No. 2, 2009
pp. 125-145

0961-5539
DOI 10.1108/09615530910930937

discontinuities in the coefficients present in the formulation and cause mathematical difficulties. To this end, computationally efficient and accurate methods are vital.

The black-oil model is particularly useful in hydrocarbon reservoir simulations as it can model both the primary and secondary hydrocarbon recovery processes. The model can feature a three-component, three-phase flow in porous media and take into account the fluid compressibility and also the mass transfer between different phases using minimum compositional data.

The set of partial differential equations, describing this model are strongly non-linear and coupled. Trangenstein and Bell (1989) showed that these equations can be written as two separate sets of inherently different partial differential equations. One set contains pressure and velocity components of the flow as its primitive variables and has a parabolic nature, whereas the other system of equations describes conservation of mass for the fluid components and has a hyperbolic nature. Although computationally intensive, the first parabolic set does not pose a great challenge to numerical methods. Numerical solution of the hyperbolic set however, requires special care because it exhibits mathematical degeneracy and its flux function is non-convex. In some situations, a particular phase may vanish, even though all chemical components are present. This situation is termed as under-saturation that leads to local linear degeneracies and loss of strict hyperbolicity in the mathematical structure of the system (Trangenstein, 1988). The loss of strict hyperbolicity poses a significant difficulty to most numerical techniques. Numerical solution of this hyperbolic system is the main focus of the current paper.

For several years, the use of Godunov-type schemes has been a natural choice to solve these complex hyperbolic equations. This is mainly due to the ability of the method to construct the flux functions by the use of characteristics thereby being able to detect the local linear degeneracy and non-strict hyperbolicity conditions. In this approach (Godunov, 1959), the numerical fluxes are determined by computing the left and right states at each cell interface, solving a local Riemann problem for these two states and evaluating the flux along the appropriate characteristics. Trangenstein (1988) presented a rather complete review on different schemes belonging to this class of methods. Osher and Solomon (1982) extended the Godunov method to solve a genuinely hyperbolic system of conservation laws. Based on their work, Bell *et al.* (1989) and Collela (1990) made modifications to a second-order form of the scheme, in order to use it in the field of oil reservoir simulation. Later, Dicks (1993) and Bergamaschi *et al.* (1998) extended the preceding schemes to two-dimensional problems with heterogeneous properties. In all these papers, the local Riemann problem is treated using Engquist–Osher (Engquist and Osher, 1980; 1981) flux estimation method, which is far less expensive than the corresponding exact Riemann-problem flux calculation. Although these methods are computationally expensive due to the use of exact eigen-structures, a stability analysis shows that this weakness can be alleviated by using relatively large time-steps (Dicks, 1993). This approach was adopted by Bell *et al.* (1989) to deal with the cases of eigenvector deficiency which arise in the complex reservoir problems.

Another important branch of numerical methods used for conservation laws is the central scheme, which has a long history in compressible flow simulation. The pioneering work of Friedrichs and Lax (1971) is known as the beginning of the central methods in which a piecewise constant approximation of the solution is used. Several attempts were made to achieve a practical method of this kind with a reasonable numerical dissipation. Recently, the method has been modified so that its numerical

dissipation is reasonably low while retaining its relative simplicity and ease of implementation. Nessyahu and Tadmor (1990) introduced a second-order successor to the Lax-Friedrichs scheme keeping the advantage of being Riemann-solver free. Their work was extended to higher orders by Liu and Tadmor (1998) and Huynh (1995) and to higher dimensions by Arminijon *et al.* (1995) and Jiang and Tadmor (1998).

In fact, the first developments of Lax-Friedrichs-based schemes for reservoir simulation including higher order formulations were presented by Edwards (2004, 2005).

Other types of high-resolution central schemes also exist. Two of the most popular central schemes are the convective-upwind split-pressure scheme due to Jameson (1995a, b) and the scheme of Liu and Osher (1998), both of which being semi-discrete and achieving high resolution without using a Riemann solver. These schemes have their main application in the field of computational aerodynamics.

The numerical dissipation of all of the above mentioned central methods is sensitive to the time-step size thus smearing discontinuities at low Courant-Friedrichs-Lewy (CFL) numbers. To remedy this deficiency, Kurganov and Tadmor (2000) recently introduced a modification to the Nessyahu–Tadmor scheme, making its numerical diffusion independent of the time-step size and of order $O(h^{2r-1})$ where h represents the mesh size and r is the order of the scheme. Another attractive aspect of this method in the field of reservoir simulation is that its semi-discrete form enables the method to handle degenerate conservation laws without using ad hoc or extra treatments (Kurganov and Tadmor, 2000). Taking advantage of this feature, Naderan *et al.* (2007) have applied three types of central schemes, one of which being the Kurganov–Tadmor scheme, to one-dimensional black-oil problems, and compared their performance in this context. In another work, the KT scheme was used for simulation of two-dimensional black oil reservoir problems by Naderan *et al.* (2006).

The accuracy of the methods become more important when there are additional sources of non-linearities in the problem. One of these cases which is of practical importance is the existence of relative permeability hysteresis, which introduces an additional history-dependent nonlinearity. This situation is particularly difficult as errors accumulate and grow significantly in time. There are various hysteresis models for relative permeability (Aziz and Settari, 1979; Killough, 1976; Carlson, 1981; Lenhard and Parker, 1987; Lenhard and Oostrom, 1998; Larsen and Skauge, 1998) with varying degrees of accuracy. Spiteri and Juanes (2004) give a comparison of the suitability of different hysteresis models from a practical point of view. In this work, a typical model proposed by Aziz and Settari (1979) is used to demonstrate the importance of accurate treatment of this effect.

In the present work, a comparison between the performance of a higher-order Godunov method and the Kurganov–Tadmor high-resolution central scheme, applied to the one-dimensional black-oil model, is carried out. Three benchmark problems each showing different aspects of the reservoir simulation problems are solved. The first test case investigates flow in a saturated reservoir. The second test case studies the ability of the two methods to handle a mixed saturated/undersaturated reservoir and the third uses a hysteresis model for the relative permeability function to simulate a complex water alternating gas (WAG) injection, a typical case of cyclic flow regime. Some of the important numerical aspects, such as the rate of convergence and the quality of discontinuity capturing with the grid spacing size are compared. In addition, the influence of reducing CFL number on the results is investigated. In the following, first a brief review of the governing equations for the black oil model is given and then details

of the numerical methods used in this work are described. Finally, the above mentioned one-dimensional benchmark problems are solved and some concluding remarks are presented.

Governing equations

Equations governing the black oil model can be formulated in several forms. The form chosen here is based on the work of Trangenstein and Bell (1989), which uses a volume error discrepancy for derivation of the pressure equation. For the sake of brevity, the details of the assumptions and derivation process are not discussed and only a brief review of the equations is presented.

In the black-oil model, the reservoir fluid is considered to be composed of three pseudo-components, which are oil, gas and water, distributed into three phases consisted of liquid, vapor and aqua. Neglecting the capillary effects, all phases have the same pressure, p. The mass of components per pore volume is represented by vector $\mathbf{z} = \{z_o, z_g, z_w\}^T$ and the volume of each phase per pore volume by $\mathbf{u} = \{u_l, u_v, u_a\}^T$. Here, subscripts o, g and w refer to the oil, gas and water components while subscripts l, v and a refer to the liquid, vapor and aqua phases, respectively. As in general u_js do not sum to one, saturations are defined as the fractions of the total fluid volume occupied by each of the three phases

$$\mathbf{s} = \frac{\mathbf{u}}{\mathbf{e}^T\mathbf{u}}, \tag{1}$$

where $\mathbf{e} = \{1, 1, 1\}^T$.

The vector of velocities is defined as

$$\mathbf{v} = \{\mathbf{v}_l, \mathbf{v}_v, \mathbf{v}_a\}^T,$$

in which, when neglecting gravitational effects,

$$\mathbf{v}_j = -\lambda_j(\nabla p), \quad j = l, v, a \tag{2}$$

are the phase velocities. Also, $\lambda_j = Kk_{r_j}/\mu_j$ is the mobility of phase j where K is the rock permeability, and k_{r_j} and μ_j are the relative permeability and dynamic viscosity of phase j, respectively.

Summing up both sides of Equation (2) for all phases gives the total velocity $\mathbf{v}_t = \mathbf{v}^T\mathbf{e} = -\lambda(\nabla p)$ where $\lambda = \sum_{j=l,v,a} \lambda_j$ is the total mobility. Defining $f_j = \lambda_j/\lambda$, the phase velocities can be written in terms of the total velocity, $\mathbf{v}_j = f_j\mathbf{v}_t$.

The equation governing pressure distribution in the domain is derived so as to correct the error in the state equation ($\mathbf{e}^T\mathbf{u} = 1$) (Trangenstein and Bell, 1989). This gives a parabolic equation in the form of

$$\left(-\phi\mathbf{e}^T\frac{\partial\mathbf{u}}{\partial p} + \mathbf{e}^T\mathbf{u}\frac{\partial\phi}{\partial p}\right)\frac{\partial p}{\partial t} + \mathbf{e}^T\frac{\partial\mathbf{u}}{\partial\mathbf{z}}\nabla\cdot(\mathbf{R}\mathbf{B}^{-1}\mathbf{v}) = \frac{\mathbf{e}^T\mathbf{u} - 1}{\Delta t}\phi \tag{3}$$

where ϕ is the porosity and t is time.

The matrix $\mathbf{B} = diag\{B_l, B_v, B_a\}$, is the volume formation factor which is the ratio of the volume of each phase at reservoir condition to the volume of the same phase at

the stock tank condition (STC). In the absence of thermal effects, Bs are only functions of the phase pressure.

The matrix $\mathbf{R}$ is the solution ratio, describing the distribution of components among phases. R_{ij} is defined as the ratio of the amount of component i in phase j to the amount of principal component of phase j. By definition, the principal component of a phase is the component present in that phase at STC. Specifically, oil, gas and water are the principal components of the liquid, vapor and aqua phases, respectively.

The model considered by Trangenstein and Bell (1989) considers the solubility of gas in both oil and water and evaporation of oil, so that

$$\mathbf{R} = \begin{bmatrix} 1 & R_v & 0 \\ R_l & 1 & R_a \\ 0 & 0 & 1 \end{bmatrix} \quad \text{with} \quad R_l = \frac{z_{gl}}{z_{ol}}, \quad R_v = \frac{z_{ov}}{z_{gv}} \quad \text{and} \quad R_a = \frac{z_{ga}}{z_{wa}} \tag{4}$$

where z_{ij} refers to the mass of component i in phase j per pore volume. In this work, the above form for $\mathbf{R}$ is adopted.

The transport of components is governed by the mass conservation law which yields

$$\frac{\partial \phi \mathbf{z}}{\partial t} + \nabla \cdot \left(\mathbf{R}\mathbf{B}^{-1}\mathbf{v} \right) = 0. \tag{5}$$

Here, the relation between $\mathbf{u}$ and $\mathbf{z}$ is given by

$$\mathbf{u} = \mathbf{B}\mathbf{T}\mathbf{z}, \tag{6}$$

where $\mathbf{T}$ is a matrix such that $\mathbf{T}\mathbf{R} = \mathbf{I}$.

When all three phases are present, the flow is termed saturated. However, there is a possibility that all of the gas content is dissolved in the liquid phase, thus, eliminating the vapor phase. This situation is called under-saturation, which shows that the reservoir pressure is higher than the liquid bubble pressure and the liquid phase has the capacity to swallow more gas. In this case, $\mathbf{R}$, $\mathbf{T}$ and $\mathbf{B}$ matrices need to be modified but the general forms of equations (3), (5) and (6) do not alter. This is the main reason for choosing this formulation as the base of the present work, since it permits a unified treatment of the saturated and under-saturated cases. For a detailed discussion of the under-saturated cases, consult (Trangenstein and Bell, 1989).

Hysteresis phenomenon

The hysteresis phenomenon corresponds to the situation when distinct curves exist for imbibition and drainage processes. This effect becomes significant in processes with strong flow reversals. Such situations occur in the case of WAG injection, in which the gas phase is trapped during water flooding after a gas flood.

The hysteresis effect can be visualized on a relative permeability diagram as shown in Figure 1 for a oil–gas system. Here, gas is the non-wetting phase while oil acts as a wetting phase. As it can be seen in this figure, the drainage curve for oil falls above the imbibition curve. If the drainage process is stopped at point A, and the process switches to the imbibition process, a path defined by AB is followed by the relative permeability of the gas phase shown here by subscript v. The figure also shows some

important parameters which are used in the modelling of this effect. The actual values used in this paper are given in appendix.

To include the hysteresis effects, the model described by Coats (Aziz and Settari, 1979) is used. All hysteresis models add some difficulties to the numerical solution of the multi-phase flow problems via introducing a history dependent non-linear function for the vapor phase relative permeability. It is emphasized that the relative permeability is the source of strong non-linearity in the black-oil model by itself.

Referring to Figure 1, the normalized relative permeability of vapor phase $\overline{k}_{rv} = k_{rv}/k_{rvro} = f(\overline{s}_v)$ is defined as a function of $\overline{s}_v$ which is given by

$$\overline{s}_v = \frac{s_v - s_{vcr}}{1 - s_{om} - s_{wc} - s_{vc}^{eff}}. \tag{7}$$

In this definition, s_{om} and s_{wc} stand for the liquid and aqua phase residual saturations and s_{vcr} is the critical vapor saturation in the drainage cycle. Also, in the definition of k_{rv}, the quantity k_{rvro} refers to k_{rv} computed at $s = 1 - s_{wc} - s_{om}$. The effective residual saturation s_{vc}^{eff} is obtained from

$$s_{vc}^{eff} = \omega s_{vc}^{*} + (1 - \omega) s_{vcr}, \tag{8}$$

where

$$\omega = \frac{s_v^A - s_v}{s_v^A - s_{vc}^{*}}, \tag{9}$$

and the current residual vapor saturation, s_{vc}^{*}, is calculated as a function of the maximum vapor saturation s_v^A reached during the drainage cycle

$$s_{vc}^{*} = s_{vc} \frac{s_v^A}{1 - s_{om} - s_{wc}}. \tag{10}$$

When s_v is increasing, ω is set to zero, $s_{vc}^{eff} = s_{vcr}$ and k_{rv} follows the original drainage curve. When s_v is decreasing, ω is set to 1 and s_{vc}^{eff} becomes s_{vc}^{*}. When s_v reaches s_{vc}^{*}, shown by point B in Figure 1, one must set $\overline{k}_{rv} = k_{rv} = 0$.

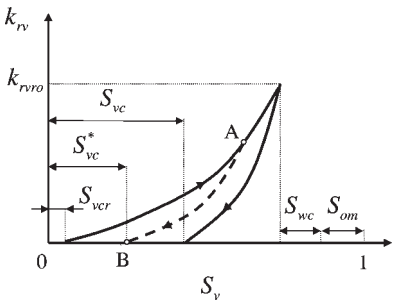

Figure 1.
Hysteresis of k_{rv} according to the Coats model

Numerical method

A finite-volume approach is used for the spatial discretization of equations (3) and (5). For a one-dimensional domain of length L, the nodal points and grid spacing are defined by

$$x_i = (i-1)\Delta x \qquad i = 1, 2, \ldots, n$$
$$\Delta x = \frac{L}{n-1}. \tag{11}$$

The control volume corresponding to node i is the region enclosed by faces $x_{i-1/2} = x_i - \Delta x/2$and $x_{i+1/2} = x_i + \Delta x/2$. Integrating equation (3) on control volume i gives

$$\iint \alpha \frac{\partial p}{\partial t} dx\, dt + \iint \mathbf{e}^T \mathbf{B}\mathbf{T} \frac{\partial}{\partial x}(\mathbf{R}\mathbf{B}^{-1}\mathbf{v}) dx\, dt = \iint \beta dx\, dt, \tag{12}$$

where

$$\alpha = -\phi \mathbf{e}^T \frac{\partial \mathbf{u}}{\partial p} + \mathbf{e}^T \mathbf{u} \frac{\partial \phi}{\partial p},$$

and

$$\beta = \frac{\mathbf{e}^T \mathbf{u} - 1}{\Delta t}\phi.$$

Assuming that p is constant over the control volume, $\mathbf{R}\mathbf{B}^{-1}$becomes independent of x, simplifying equation (12) as

$$\alpha_i (p_i^{n+1} - p_i^n)\Delta x + \Delta t \left[(v_t^{n+1})_{i+1/2} - (v_t^{n+1})_{i-1/2} \right] = \beta_i \Delta x \Delta t \tag{13}$$

The coefficients α and β are evaluated at time t_n while the total velocities are evaluated at time t_{n+1}, resulting in an implicit equation for pressure. Note also that the vector notation for the total velocity is not required any more as the equation is written in one dimension.

The above implicit equation can be solved in various ways. Here, a relaxation method is adapted. To do so, $p_i^{n+1,k}$is defined as the kth iteration value for p_i^{n+1}. Defining the residual of the discretized equation in iteration k as

$$res_i^k = \alpha_i (p_i^{n+1,k} - p_i^n)\Delta x + \Delta t \left[(v_t^{n+1,k})_{i+1/2} - (v_t^{n+1,k})_{i-1/2} \right] - \beta_i \Delta x \Delta t, \tag{14}$$

the iteration formula for pressure becomes

$$p_i^{n+1,k+1} = p_i^{n+1,k} - \omega (res)_i^k, \tag{15}$$

in which ω is the relaxation factor. Numerical experiments showed that a value $\omega = 1.1$ yields a good compromise between the convergence rate and stability though it might

not be an optimum value. Interface velocities $v_{t,i+1/2}^{n+1,k}$ are calculated by discretizing the total velocity equation as

$$v_{t,i+1/2}^{n+1,k} = -\lambda_{i+1/2} \frac{p_{i+1}^{n+1,k} - p_i^{n+1,k}}{\Delta x}. \tag{16}$$

To deal with non-linearities, $\lambda_{i+1/2}$ is calculated using harmonic averaging as

$$\lambda_{i+1/2} = \frac{2\lambda_i \lambda_{i+1}}{\lambda_i + \lambda_{i+1}}. \tag{17}$$

It is assumed that convergence is achieved for the non-linear iteration loop when $\|res^k\| \leq 10^{-6}$. The computed pressure field is then used for the rest of calculations within the time-step.

For the component transport, integration over the control volume using an explicit time approximation gives

$$\mathbf{z}_i^{n+1} - \mathbf{z}_i^n = -\frac{\Delta t}{\phi_i \Delta x} [\mathbf{h}_{i+1/2} - \mathbf{h}_{i-1/2}] \tag{18}$$

where $\mathbf{h}_{i\pm1/2}$ is the flux vector $\mathbf{RB}^{-1}\mathbf{v}$ evaluated at the interface $i \pm 1/2$. $\mathbf{h}$ can be written as a function of the conserved variables on the two sides of the interface. The above explicit formulation results in the first-order methods in time. Below, two flux estimation techniques used in this work are presented. The general solution algorithm is shown in Figure 2.

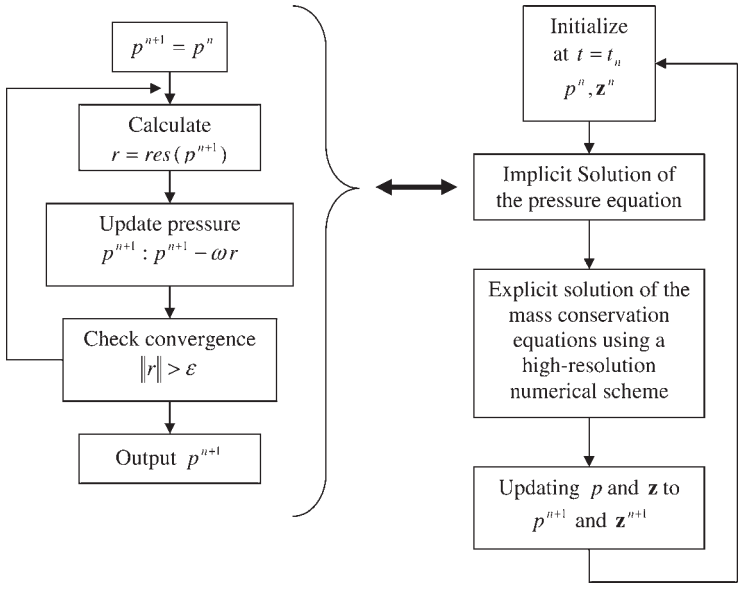

Figure 2.
Flowchart of the solution algorithm

The *CFL* condition for the numerical methods used in this work is computed on the basis of the maximum wave speed, λ_{max}, and a global *CFL* number, *C*, at each face, using

$$\frac{\lambda_{max}\Delta t}{\Delta x} < C. \tag{19}$$

Kurganov–Tadmor scheme

The KT method is a higher-order central scheme based on averaging over the non-smooth Riemann fans. Unlike most of the other Lax–Friedrichs-based schemes which use a one-stage reconstruction process, the KT method consists of two linear reconstruction stages. First, new cell average values are computed on a nonuniform staggered grid. The values are then used to advance the solution in time. Finally, in the second stage, the solution is converted back into the original computational grid. One advantage of the KT method over the Nessyahu and Tadmor (1990) is that it avoids the use of associated staggered grids. Another major advantage of the KT method is that it separates the treatment of smooth and non-smooth regions of the solution thereby generating less numerical diffusion. This is achieved by using staggered cells, which are just large enough for Riemann fans to propagate inside the domain of averaging. In most Lax–Friedrichs-based schemes, this is not the case and as a result, it is assumed that the discontinuity propagated from the cell interface has swept the whole region of integration. When this assumption is violated, excessive numerical dissipation are introduced into the solution especially near discontinuities and rarefaction tips.

Kurganov and Tadmor formulated their scheme in both semi and fully-discrete forms. Here, the semi-discrete form is used since it is already in the conservation form. Nevertheless, the same expression for face flux can be obtained from the fully-discrete form with some algebraic manipulations. This method has an artificial diffusion of order $O(\Delta x^3)$ and its numerical flux is given by Kurganov and Tadmor (2000)

$$\mathbf{h}_{i+1/2} = \frac{1}{2}[\mathbf{h}^{+}_{i+1/2} + \mathbf{h}^{-}_{i+1/2}] - \frac{1}{2}a_{i+1/2}(\mathbf{z}^{+}_{i+1/2} - \mathbf{z}^{-}_{i+1/2}) \tag{20}$$

in which $\mathbf{z}^{+}_{i+1/2} = \mathbf{z}_{i+1} - \Delta x/2\mathbf{z}_{x,i+1}$, and $\mathbf{z}^{-}_{i+1/2} = \mathbf{z}_i + \Delta x/2\mathbf{z}_{x,i}$ are the right and left states, respectively, and $\mathbf{h}^{\pm}_{i+1/2} = \mathbf{h}(\mathbf{z}^{\pm}_{i+1/2})$. The variable derivatives are evaluated as follows:

$$\mathbf{z}_{x,i} = minmod\Big(\frac{\mathbf{z}_{i+1} - \mathbf{z}_i}{\Delta x}, \frac{\mathbf{z}_i - \mathbf{z}_{i-1}}{\Delta x}\Big),$$

$$\mathbf{z}_{x,i+1} = minmod\Big(\frac{\mathbf{z}_{i+2} - \mathbf{z}_{i+1}}{\Delta x}, \frac{\mathbf{z}_{i+1} - \mathbf{z}_i}{\Delta x}\Big),$$

where the *minmod* limiter is defined as

$$minmod(x,y) = \begin{cases} min(x,y) & x > 0 \text{ and } y > 0 \\ max(x,y) & x < 0 \text{ and } y < 0 \\ 0 & xy < 0 \end{cases} \tag{21}$$

Also, $a_{i+1/2}$ is the spectral radius of $\partial\mathbf{h}/\partial\mathbf{z}$ with $\mathbf{z} \in \mathscr{C}(\mathbf{z}^{-}_{1+1/2}, \mathbf{z}^{+}_{1+1/2})$ where $\mathscr{C}$ is a path that connects the two states $\mathbf{z}^{-}_{i+1/2}$ and $\mathbf{z}^{+}_{i+1/2}$ in the phase space via Riemann fans.

Since the flux function is non-convex and complicated to evaluate, it is not easy to find $a_{i+1/2}$ accurately. Dicks (1993) used the arithmetic mean of the left and right states to approximate the eigenvalues between the two states, as suggested by Bell *et al.* (1989). This approximation is used here to calculate the spectral radius of $\partial\mathbf{h}/\partial\mathbf{z}$ which is used as an estimate for $a_{i+1/2}$, in order to be consistent with the higher order Godunov scheme, described later. Numerical experiments showed that this is sufficiently close to the actual maximum wave speed.

Kurganov and Tadmor (2000) recovered the Rusanov scheme which is a first-order method by setting the extrapolation slopes (i.e. $\mathbf{z}_{x,i}$ and $\mathbf{z}_{x,i+1}$) in their computations equal to zero. They showed the results obtained by this first-order version in some of their test cases and concluded that in some cases it performs better than the second-order Nessyahu–Tadmor scheme. However, in all their tests and specially in strongly degenerate ones, their second-order scheme outperformed both the Rusanov and Nessyahu–Tadmor schemes.

For a more elaborate description of the above method consult Kurganov and Tadmor (2000). Also, a detailed description of the method for solving reservoir problems using the Black-oil model was given in reference Naderan *et al.* (2007).

Higher order Godunov scheme

An alternative approach to solve the conservation equation (18) is the use of a higher order Godunov-based scheme. Below a higher order Godunov scheme for such a system of equations is presented. Beginning with a piecewise constant approximation for $\mathbf{z}$ within each computational cell, the "centered", "left" and "right" slopes (variation of $\mathbf{z}$ per unit variation of x) are computed. These slopes are expanded in terms of the right eigenvectors $\mathbf{r}_k$ of the Jacobian matrix $\partial\mathbf{h}/\partial\mathbf{z}$, as

$$\begin{aligned} \frac{1}{2}(\mathbf{z}_{j+1} - \mathbf{z}_{j-1}) &= \sum_{k=1}^{m} \alpha^{c}_{k}\mathbf{r}_k, \\ \mathbf{z}_{j+1} - \mathbf{z}_{j} &= \sum_{k=1}^{m} \alpha^{r}_{k}\mathbf{r}_k, \\ \mathbf{z}_{j} - \mathbf{z}_{j-1} &= \sum_{k=1}^{m} \alpha^{l}_{k}\mathbf{r}_k, \end{aligned} \tag{22}$$

where m is the number of equations. To construct a second-order method, an approximation to the slope $\partial\mathbf{z}/\partial x$ is needed which must be monotonized in order to prevent oscillations near discontinuities. Such a monotonized slope is defined by

$$\Delta\mathbf{z} = \sum_{k=1}^{m} \alpha_k \mathbf{r}_k, \tag{23}$$

where the expansion coefficients from equation (22) are "limited" to give

$$\alpha_k = \begin{cases} \min(|\alpha^{c}_{k}|, \gamma|\alpha^{l}_{k}|, \gamma|\alpha^{r}_{k}|)\mathrm{sign}(\alpha^{c}_{k}), & \text{if } \alpha^{r}_{k}\alpha^{l}_{k} > 0 \\ 0, & \text{otherwise} \end{cases} \tag{24}$$

in which γ is a constant parameter, introduced by Van Leer (1979) and is usually set to 2. It should be noticed that using this value, in regions of smooth flow, $\Delta\mathbf{z}$ is given by centered differences, whereas near extreme points, $\Delta\mathbf{z}$ is set to zero.

The left and right states at the grid cell interfaces are computed according to Dicks (1993)

$$\mathbf{z}^L_{j+1/2} = \mathbf{z}^n_j + \frac{1}{2}R_j\left(I - \frac{\Delta t}{\Delta x}\Lambda_j\right)\alpha_j, \tag{25}$$

$$\mathbf{z}^R_{j+1/2} = \mathbf{z}^n_{j+1} - \frac{1}{2}R_{j+1}\left(I + \frac{\Delta t}{\Delta x}\Lambda_{j+1}\right)\alpha_{j+1}, \tag{26}$$

where Λ is the diagonal matrix of eigenvalues of $\mathbf{H}$ and R is its respective matrix of eigenvectors.

Exploiting these left and right states, a Riemann problem at the cell interface is solved. This is achieved using a generalization of the Engquist–Osher numerical flux (Engquist and Osher, 1980, Engquist and Osher, 1981). First a path is constructed from $\mathbf{z}^L$ to $\mathbf{z}^R$ that approximates the phase space solution to the Riemann problem, and then a numerical flux is computed. The approximate phase space solution could be considered as a decomposition of the jump from $\mathbf{z}^L$ to $\mathbf{z}^R$ into m jumps corresponding to each of the wave modes. To achieve such a decomposition, first an expansion state as the average of the left and right states, $\bar{\mathbf{z}} = \frac{1}{2}(\mathbf{z}^L + \mathbf{z}^R)$ is calculated and then the generalized eigenvectors at this state are evaluated as $\bar{R}_k = \mathbf{r}_k(\bar{\mathbf{z}})$. The jump between two states $\mathbf{z}^L$ and $\mathbf{z}^R$ can be decomposed in terms of linearly independent vectors $\bar{R}_k$. Using this decomposition, $m-1$ intermediate states between $\mathbf{z}^L$ and $\mathbf{z}^R$ can be formed as

$$\mathbf{z}_k = \mathbf{z}^L + \sum_{i=1}^{k} \bar{\alpha}_i \bar{\mathbf{R}}_i, \quad 1 \le k < m \tag{27}$$

where each of them is related to a wave mode. In the Engquist–Osher (EO) method, the numerical flux is written as a flux at a reference state plus an integral correction term. First, the mean speed is defined as

$$\sigma = \frac{(\mathbf{h}(\mathbf{z}^L) - \mathbf{h}(\mathbf{z}^R)) \cdot (\mathbf{z}^L - \mathbf{z}^R)}{\|\mathbf{z}^L - \mathbf{z}^R\|^2} \tag{28}$$

and the reference state is given by

$$\mathbf{z}^{\text{ref}} = \begin{cases} \mathbf{z}^L, & \text{if } \sigma \ge 0 \\ \mathbf{z}^R, & \text{otherwise} \end{cases} \tag{29}$$

The above choice of reference state is equivalent to using an upwind direction and the sign of σ is a measure of the sign of eigenvalues of matrix $\mathbf{H}$. Finally, the approximate EO flux at both reference states depending on upwind direction is calculated according to

$$\mathbf{h}^{EO}(\mathbf{z}^L, \mathbf{z}^R) = \mathbf{h}(\mathbf{z}^L) + \sum_{k=1}^{m} \left(\int_0^{\bar{\alpha}_k} \min(\bar{\lambda}_k, 0) d\alpha \right) \bar{R}_k \tag{30}$$

or

$$\mathbf{h}^{EO}(\mathbf{z}^L, \mathbf{z}^R) = \mathbf{h}(\mathbf{z}^R) - \sum_{k=1}^{m} \left(\int_0^{\bar{\alpha}_k} \max(\bar{\lambda}_k, 0) d\alpha \right) \bar{R}_k \tag{31}$$

Here, $\bar{\lambda}_k$ is an approximation to the wave speed along the line segments $\bar{\Gamma}_k$ which are defined as the paths from $\mathbf{z}_{k-1}$ to $\mathbf{z}_k$ that altogether cover the whole path from $\mathbf{z}^L$ to $\mathbf{z}^R$. The preceding integrals are computed by representing the wave speeds, $\bar{\lambda}_k$, as cubic polynomial interpolation along the path $\bar{\Gamma}_k$. A cubic polynomial is needed in order to consider the inflection points in the physical flux function.

In the black-oil model, the system of mass conservation equations may exhibit lack of strict hyperbolicity and genuine non-linearity, which can be treated by adding an extra numerical dissipation term as described in detail by Bell *et al.* (1989).

Test cases

To assess the performance of the above mentioned numerical methods, three test cases are studied. For each test, the results obtained using both the Higher order Godunov (HG) and the Kurganov–Tadmor (KT) methods are shown. All fluid and rock properties were taken from Trangenstein and Bell (1989), and are given in appendix. All test cases solved in this paper are one-dimensional. A comparative study on the performance and accuracy of the HG and KT methods in two-dimensional problems with and without gravity effect can be found in (Naderan *et al.* 2006). Also, Edwards (2004, 2005) has investigated the performance of the Lax-Friedrichs-based schemes when eigenvalues change sign in two-dimensional problems involving gavity.

The first test case involves injection of a saturated mixture into a saturated reservoir. The initial reservoir pressure is 1,800 psi, whereas injection and production take place at 2,000 and 1,600 psi, respectively. This test case signifies the effect of composition variation on the flow. The computational domain is set to $0 \leq x \leq 1{,}000$ ft and the initial reservoir and injection compositions are

$$\mathbf{z}_{res} = \begin{Bmatrix} 0.703 \\ 70.3 \\ 0.0502 \end{Bmatrix}, \quad \mathbf{z}_{inj} = \begin{Bmatrix} 0.0414 \\ 66.23 \\ 0.497 \end{Bmatrix}. \tag{32}$$

The second test case is the water flooding in an under-saturated oil reservoir. The initial, injection and production pressures are 3,500, 4,000 and 3,000 psi, respectively. This test case shows the effect of pressure variation on the flow and composition. The domain is the same as the first test case and the initial reservoir and injection compositions are

$$\mathbf{z}_{res} = \begin{Bmatrix} 0.646 \\ 116.29 \\ 0.0 \end{Bmatrix}, \quad \mathbf{z}_{inj} = \begin{Bmatrix} 0.0 \\ 0.0 \\ 1.27 \end{Bmatrix}. \tag{33}$$

Both of these benchmark problems were taken from Trangenstein and Bell (1989). It should be emphasized that the results obtained by HG method are virtually the same as those shown in reference Trangenstein and Bell (1989), therefore the results were labelled as the HG results.

The third test case is a WAG injection and aims at assessing the performance of the schemes in a much more complex flow regime. The problem consists of three cycles of water-gas injection, where each cycle consists of injection of water, followed by injection of gas, with each injection having a period of 90 days. The computational domain and the initial, injection and production pressures are the same as the second test case. The initial reservoir and injection compositions are

$$\mathbf{z}_{res} = \begin{Bmatrix} 0.761 \\ 0.0 \\ 0.393 \end{Bmatrix}, \quad \mathbf{z}_{inj}, w = \begin{Bmatrix} 0.22 \\ 0.0 \\ 1.097 \end{Bmatrix}, \quad \mathbf{z}_{inj}, g = \begin{Bmatrix} 0.0625 \\ 166.17 \\ 0.303 \end{Bmatrix}, \tag{34}$$

where $\mathbf{z}_{inj}, w$ and $\mathbf{z}_{inj}, g$ refer to composition of injected fluid in water and gas injection cycles, respectively.

This test case involves alternating flow in which hysteresis effect in the relative permeability curves plays an important role. This makes the test case a history dependent and highly nonlinear problem, in which any small initial error leads to a significant difference in the final result. To account for hysteresis, the model described by Aziz and Settari (1979) is used and its parameters are given in appendix.

Results and discussion

Test case 1

For this test case, no analytical solution exists. Trangenstein and Bell (1989) showed that the solution consists of two wave fronts, one slow-running wave between the oil and water components and one fast-running wave between the gas and oil components. The problem was solved on four grids with 50, 100, 200 and 400 nodes to examine the mesh dependency of each method with a CFL number of $C = 0.45$ for the KT method and $C = 0.9$ for the HG method. In practice, these translate to the minimum and maximum time-step sizes about $\Delta t = 0.05$ (days) and 0.25 (days), respectively.

The results of computed saturation profiles are shown in Figure 3 after $t = 150$ days injection. As it can be seen, there is a rarefaction starting at $x = 50$ ft, continuing up to a shock at $x = 150$ ft indicating the presence of a local linear degeneracy due to existence of a slower wave speed which is resolved more sharply by the HG method, even though both methods predict roughly the same shock strength. Further downstream, the faster wave mode forms a rarefaction at $x = 425$ ft, connecting to a shock at $x = 725$ ft. Again the solution by the HG method is a bit sharper as a result of exact calculation of eigenvalues in contrast to the KT method that considers only one typical approximate wave speed for all phases denoted by a, as mentioned earlier. It is also noticeable that as the grid is refined the HG method converges to a mesh-independent solution more rapidly than the KT method. The resolution of the HG with 100 grid points is acceptable while the KT method reaches to a suitable accuracy by using 200 grid points.

Test case 2

Like the previous test case, there is no analytical solution for this test case. As expected the solution exhibits, a front between water and oil which starts from the injection well

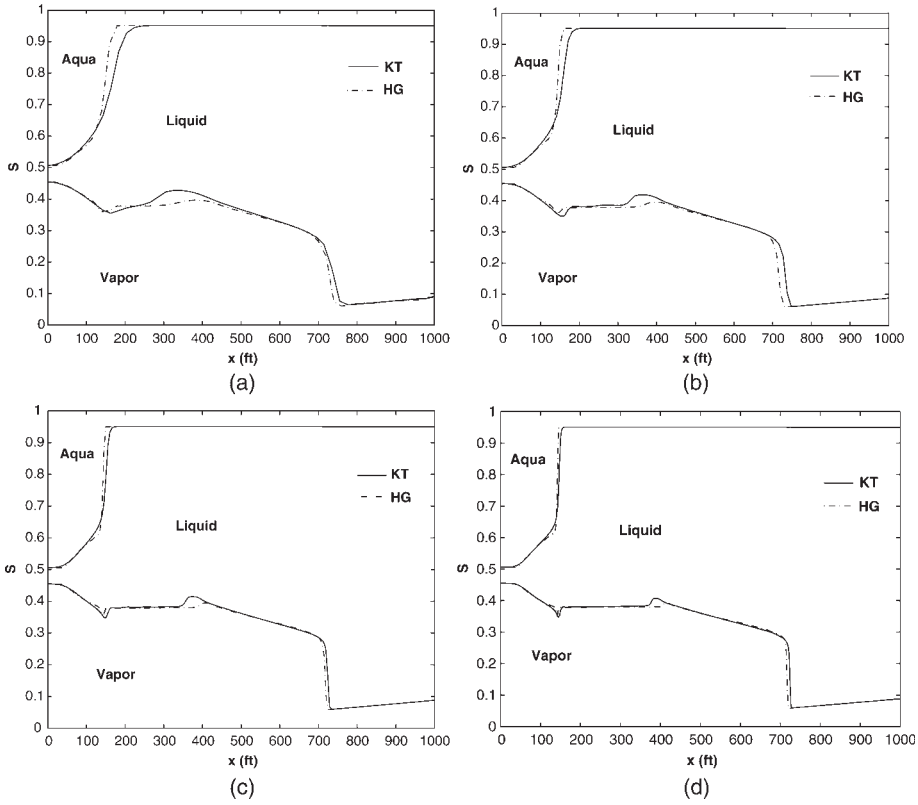

Figure 3.
Test case 1: saturation profiles after 150 days for various number of grid points: (a) 50, (b) 100, (c) 200 and (d) 400 points

and progresses towards the production well. As the reservoir pressure drops, near the production well, the flow becomes saturated and free gas is produced, which introduces another front.

Results (Figure 4) show that, there is a contact rarefaction shock pattern due to existence of a faster running wave. The rarefaction-shock pattern is resolved with approximately the same accuracy by both methods, while the HG method exhibits a better accuracy in resolving the contact discontinuity. This is due to the fact that calculation of the eigen-structure by the HG method is more accurate. Again, it is seen that the HG method converges faster to a mesh-independent solution.

With regard to the sensitivity of the methods to CFL reduction, it was shown in reference Naderan *et al.* (2007) that the KT method is virtually unaffected by the variations in CFL number. A similar test was conducted for the HG method in the present work and the results confirmed that the same is true for this method. Hence, it can be concluded that both methods are equally insensitive to the reduction of CFL number.

Test case 3

In this test case, the capability of both KT and HG methods in capturing complex features occurring in the reservoir is examined. As it was mentioned before, in this test case the hysteresis effect is considered and the injection of water and gas is performed in alternating stages. The result of simulations are shown in Figures 5, 6 and 7. It is

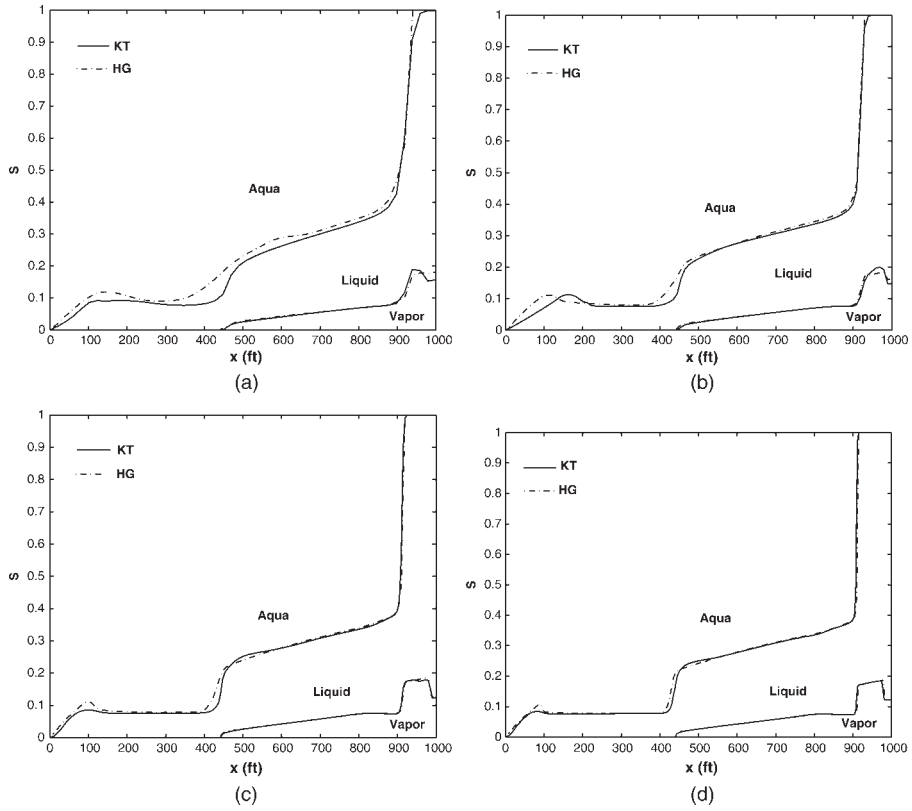

Figure 4.
Test case 2: saturation profiles after 125 days for various number of grid points: (a) 50, (b) 100, (c) 200 and (d) 400 points

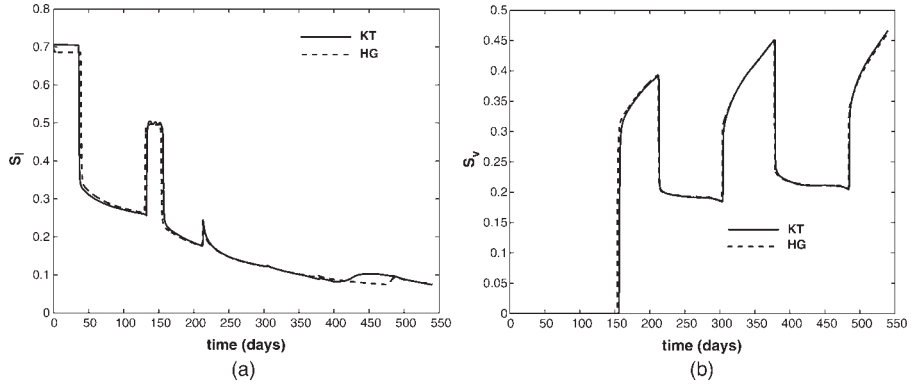

Figure 5.
Test case 3: variation of saturation profiles at $x = 250$ ft with time: (a) liquid phase and (b) vapor phase

remarkable that the results obtained by the HG and KT methods are very close to each other even in the regions with sharp gradients.

The variation of liquid and vapor phase saturations with time for a point inside the reservoir ($x = 250$ ft) is shown in Figure 5. As can be seen, there are three humps in this

profile indicating three stages of gas injection. It is also noticed that due to gas trapping effect the peak of consecutive injection stages increases for the gas phase and decreases for the liquid phase.

The results shown in Figure 6 corresponds to the saturation profile of the three phases across the reservoir at $t = 246$ days and $t = 350$ days. These profiles exhibit the propagation of injected water and gas fronts, pushing the oil resident in reservoir, towards the production well. It is noticeable that the accuracy of both the KT and HG methods are comparable in capturing sharp fronts and discontinuities.

Finally, in Figure 7 the effect of WAG on the sweep efficiency and oil cut curves are shown. The sweep efficiency is defined as the ratio of extracted oil to the total amount of oil in place and the oil cut curve is indicative of the fraction of oil in the extracted reservoir fluid. From these curves, it is evident that for the WAG injection process modelled here, there is a close agreement between the KT and HG methods.

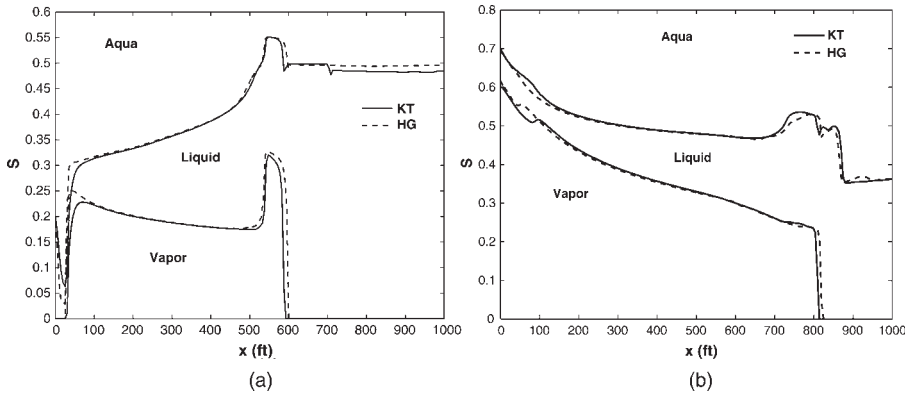

Figure 6.
Test case 3: saturation profiles along reservoir: (a) after 246 days and (b) after 350 days

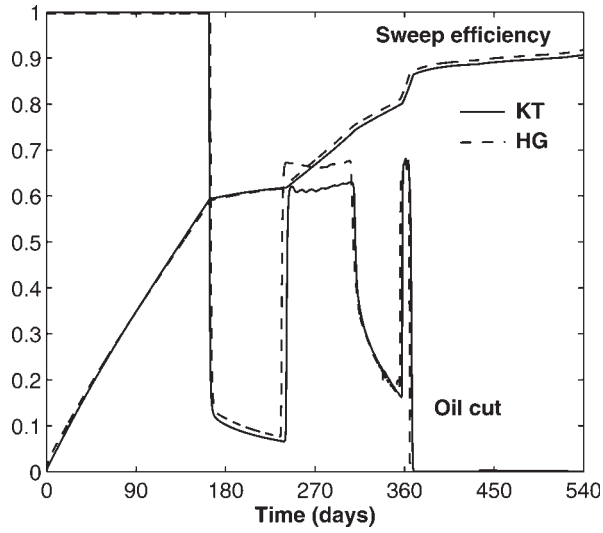

Figure 7.
Test case 3: sweep efficiency and oil cut curves

Conclusion

In this work, a comparative study between two types of high-resolution numerical methods were presented to study black-oil problems in one dimension. It was shown that both the KT and HG methods can produce accurate results for all test case studied in this work and appropriately handle complex mathematical features such as linear degeneracy and loss of hyperbolicity. The methods also performed well in solving a problem involving hysteresis effect.

The higher order Godunov method however, gives more accurate results particularly near discontinuities and converges faster to a mesh-independent solution. This can be attributed to the calculation of eigen-structure in an exact fashion. On the other side, the KT scheme proves to be a viable scheme for practical purposes mainly due to its relatively simpler formulation, ease of implementation and acceptable accuracy.

References

Arminijon, P., Stanescu, D. and Viallon, M.C. (1995), "A two-dimensional finite volume extension of the Lax–Friedrics and Nessyahu–Tadmor schemes for compressible flow", in Hafez, M. (Ed.) *Proceedings of the 6th International Symposium on CFD, Lake Tahoe*, Vol. 4, pp. 7-14.

Aronofsky, J.S. and Jenkins, R. (1954), "A simplified analysis of unsteady radial gas flow", *Transactions of AIME*, Vol. 201, pp. 149-54.

Aziz, K. and Settari, A. (1979), "Petroleum reservoir simulation", *Applied Science*, London.

Bell, J.B., Collela, P. and Trangenstein, J.A. (1989), "High-order Godunov methods for general systems of hyperbolic conservation laws", *Journal of Computational Physics*, Vol. 82, pp. 362-97.

Bergamaschi, L., Mantica, S. and Manzini, G. (1998), "A mixed finite element-finite volume formulation of the black-oil model", *SIAM Journal of Scientific Computing*, Vol. 20, pp. 970-97.

Carlson, F.M. (1981), "Simulation of relative permeability hysteresis to the nonwetting phase", SPE paper 10157, SPE Annual Technical Conference and Exhibition, San Antonio, TX.

Class, H., Helmig, R. and Bastian, P. (2002), "Numerical simulation of non-isothermal multiphase multicomponent processes in porous media", *Advances in Water Resources*, Vol. 25 No. 5, pp. 533-50.

Collela, P. (1990), "Multidimensional upwind methods for hyperbolic conservation laws", *Journal of Computational Physics*, Vol. 87, pp. 171-200.

Dicks, M.E. (1993), "Higher order Godunov Black-oil simulations for compressible flow in porous media", PhD thesis, University of Reading, Reading.

Edwards, M.G. (2004), "Non-upwind monotonicity based finite volume schemes for hyperbolic conservation laws in porous media", *Proceedings of 9th European Conference on Mathematics of Oil Recovery, Cannes, France, 30 August-2 September 2004*.

Edwards, M.G. (2005), "Non-upwind versus upwind schemes for hyperbolic conservation laws in porous media", *Proceedings of SPE Reservoir Simulation Symposium, paper: spe93691, Houston, TX, February 2005*.

Engquist, B. and Osher, S. (1980), "Stable and entropy satisfying approximations for transonic flow calculations", *Mathematics of Computation*, Vol. 34, pp. 45-75.

Engquist, B. and Osher, S. (1981), "One sided difference approximations for nonlinear conservation laws", *Mathematics of Computation*, Vol. 36, pp. 321-51.

Friedrichs, K.O. and Lax, P.D. (1971), "Systems of conservation equations with a convex extension", *Proceedings of the National Academy of Sciences of United States of America*, Vol. 68, pp. 1686-8.

Ghafouri, H.R. and Lewis, R.W. "A finite element double porosity model for heterogeneous deformable porous media", *International Journal for Numerical and Analytical Method in Geomechanics*, Vol. 20, pp. 831-44.

Godunov, K.S. (1959), "A finite difference method for the numerical computation of discontinuous solutions of the equations of fluid dynamics", *Math Sbornik*, Vol. 47, pp. 271-90.

Huynh, H.T. (1995), "A piecewise-parabolic dual-mesh method for the Euler equations", 12th AIAA Computational Fluid Dynamics Conference, pp. 1054-66.

Jameson, A. (1995a), "Analysis and design of numerical schemes for gas dynamics 1 – artificial diffusion, upwind biasing, limiters and their effect on accuracy and multigrid convergence", *International Journal of Computational Fluid Dynamics*, Vol. 4, pp. 171-218.

Jameson, A. (1995b), "Analysis and design of numerical schemes for gas dynamics 2 – artificial diffusion and discrete shock structure", *International Journal of Computational Fluid Dynamics*, Vol. 5, pp. 1-38.

Jiang, G.S. and Tadmor E. (1998), "Nonoscillatory central schemes for multidimensional hyperbolic conservation laws", *SIAM Journal of Scientific Computing*, Vol. 19, pp. 1892-917.

Killough, J.E., (1976), "Reservoir simulation with history-dependent saturation functions", *SPE Journal Transaction of AIME*, Vol. 261, pp. 37-48.

Kurganov, A. and Tadmor, E. (2000), "New high-resolution central schemes for nonlinear conservation laws and convection-diffusion equations", *Journal of Computational Physics*, Vol. 160, pp. 241-82.

Larsen, J.A. and Skauge, A. (1998), "Methodology for numerical simulation with cyclic-dependent relative permeabilities", *SPE Journal*, Vol. 3 No. 2, pp. 163-73.

Lenhard, R.J. and Parker, J.C. (1987), "A model for hysteretic constitutive relations governing multiphase flow, 2. Permeability-saturation relations", *Water Resources Research*, Vol. 23 No. 12, pp. 2197-206.

Lenhard, R.J. and Oostrom, M. (1998), "A parametric model for predicting relative permeability-saturation-capillary pressure relationships of oilwater systems in porous media with mixed wettability", *Transport in Porous Media*, Vol. 31, pp. 109-31.

Lewis, R.W. and Sukirman, Y. (1993), "Finite element modelling of three- phase flow in deforming saturated oil reservoirs", *International Journal for Numerical and Analytical Methods in Geomechanics*, Vol. 17, pp. 577-98.

Liu, X.D. and Osher, S. (1998), "Convex ENO high order multi-dimensional schemes without field by field decomposition or staggered grids", *Journal of Computational Physics*, Vol. 160, p. 304.

Liu, X.D. and Tadmor, E. (1998), "Third order nonoscillatory central scheme for hyperbolic conservation laws", *Numerical Mathematics*, Vol. 79, pp. 397-425.

Naderan, H., Manzari, M.T. and Hannani, S.K. (2006), "Simulation of three phase flow in porous media using a high resolution central scheme", *Proceedings of the European Conference on Computational Fluid Dynamics (ECCOMAS CFD), Netherlands, 5-8 September*.

Naderan, H., Manzari, M.T. and Hannani, S.K. (2007), "Application and performance comparison of high resolution central schemes for black oil model", *International Journal of Numerical Methods for Heat and Fluid Flow*, Vol. 17 No. 7, pp. 736-53.

Nessyahu, H. and Tadmor, E. (1990), "Non-oscillatory central differencing for hyperbolic conservation laws", *Journal of Computational Physics*, Vol. 87, pp. 408-63.

Osher, S. and Solomon, F. (1982), "Upwind difference scheme for hyperbolic systems of conservation laws", *Mathematics and Computation*, Vol. 38, pp. 339-74.

Pao, W.K.S. and Lewis, R.W. (2002), "Three-dimensional Finite element simulation of three-phase flow in a deforming fissured reservoir", *Computational Methods Applied in Mechanical Engineering*, Vol. 191, pp. 2631-59.

Spiteri, E. and Juanes, R. (2004), "Impact of relative permeability hysteresis on numerical simulation of WAG injection", *Journal of Petroleum Science and Engineering*, Vol. 50, pp. 115-39.

Trangenstein, J.A. and Bell, J.B. (1989), "Mathematical structure of the black-oil model for petroleum reservoir simulation", *SIAM Journal of Applied Mathematics*, Vol. 49 No. 3, pp. 749-83.

Trangenstein, J.A. (1988), "Multiphase flow in porous media: mechanics, mathematics, and numerics', *Lecture Notes in Engineering*, Vol. 34, Springer-Verlag, New York, NY.

Van Leer, B. (1979), "Towards the ultimate conservative difference scheme. V. A second order sequel to Godunov's method", *Journal of Computational Physics*, Vol. 32, pp. 101-36.

Watts, J.W. (1997), "Reservoir simulation: past, present and future", *SPE Journal of Computer Applications*, Vol. 9 No. 6, pp. 171-6.

Appendix

Properties of rock and fluids

The spatial coordinate x has units of feet, and time t is measured in days. Pressure p is measured in psi, viscosity in centipoise and the rock permeability K is measured in 0.006328 times the value in milliDarcies. In this work, $K = 100$ md and porosity is given by $\phi = 0.2(1 + 10^{-5}p)$.

The relative permeability functions used in the first and second test cases are

$$k_{r_l} = (1 - s_v - s_a)(1 - s_v)(1 - s_a)$$
$$k_{r_v} = s_v^2$$
$$k_{r_a} = s_a^2$$

But in hysteresis model, by consideration of residual saturations the normalized form of Stone's first model proposed by Aziz and Settari (1979) is preferred that is depicted in Figure A1.

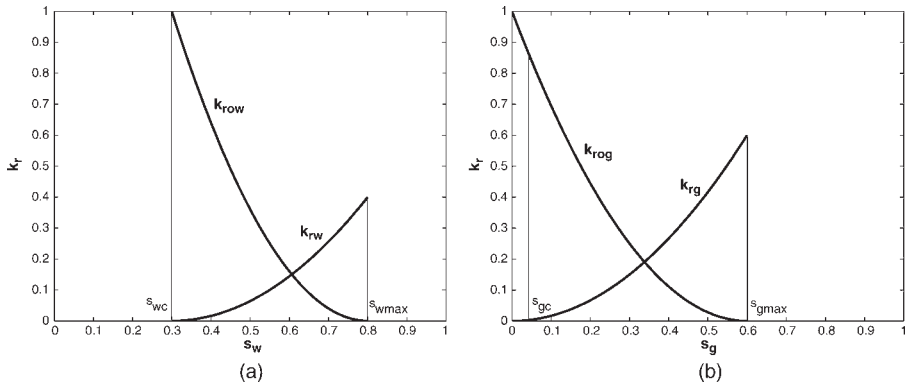

Figure A1. Relative permeability curves in a two phase: (a) oil-water system and (b) gas-oil system

The solution ratios are given as

$$R_l(p) = 0.05p$$
$$R_v(p) = 9 \times 10^{-5} - 6 \times 10^{-8}p + 1.6 \times 10^{-11}p^2$$
$$R_a(p) = 0.005p$$

Viscosities are defined by

$$\mu_l = \begin{cases} 0.8 - 10^{-4}p & \text{saturated liquid} \\ (0.8 - 10^{-4}p_b) & \\ \quad (1 + 6.78 \times 10^{-5}(p - p_b)) & \text{under - saturated liquid} \end{cases}$$

$$\mu_v = 0.012 + 3 \times 10^{-5}p$$

$$\mu_a = \begin{cases} 0.35 & \text{saturated aqua} \\ 0.35(1 + 6.78 \times 10^{-5}(p - p_b)) & \text{under - saturated aqua} \end{cases}$$

where p_b denotes bubble pressure and the volume formation factors are

$$B_l = \begin{cases} 1.0 - 2.31 \times 10^{-5}p & \text{if} R_l(p) \equiv 0 \\ 1.0 + 1.5 \times 10^{-4}p & \text{saturated liquid} \\ \dfrac{1.0 + 1.5 \times 10^{-4}p_b}{1.0 + 2.31 \times 10^{-5}(p - p_b)} & \text{under - saturated liquid} \end{cases}$$

$$B_v = \begin{cases} \dfrac{1}{6.0 + 0.06p} & \text{saturated vapor} \\ \dfrac{1}{7.0 + 0.06p} + \dfrac{\bar{R}_v}{R_v} & \\ \quad \left(\dfrac{1}{6.0 + 0.06p} - \dfrac{1}{7.0 + 0.06p}\right) & \text{under - saturated vapor} \end{cases}$$

$$B_a = \begin{cases} 1.0 - 1.8 \times 10^{-5}p & \text{if } R_a(p) \equiv 0 \\ 1.0 - 3 \times 10^{-6}p & \text{saturated aqua} \\ \dfrac{1.0 - 3 \times 10^{-6}p_b}{1.0 + 1.8 \times 10^{-5}(p - p_b)} & \text{under - saturated aqua} \end{cases}$$

where $\bar{R}_v$ is volatile oil ratio. Finally, the empirical parameters of the hysteresis phenomenon are given as

$$
\begin{aligned}
s_{wc} &= 0.3 \\
s_{w\max} &= 0.8 \\
s_{om} &= 0.05 \\
s_{gc} &= 0.3 \\
s_{g\max} &= 0.6 \\
s_{vcr} &= 0.0 \\
k_{r\mathrm{wm}} &= 0.4 \\
k_{rgm} &= 0.6 \\
k_{rocw} &= 1.0
\end{aligned}
$$